Poster contributions of the "Advanced Lectures on the Starburst-AGN Connection", Eds. R. Mújica, I. Aretxaga & D. Kunth, 2001, INAOE Electronic Edition (http://www.inaoep.mx/∼agn00/posters.html), pp. 51-54

Star Formation Activities in Narrow-Line Seyfert 1 Galaxies

T. Kawaguchi[1] **and K. Aoki**[2]

[1] Department of Astronomy, Graduate School of Science, Kyoto University, Kyoto 606-8502, Japan
[2] Astronomical Data Analysis Center, National Astronomical Observatory of Japan, Mitaka, Tokyo 181-8588, Japan

Abstract. With 144 Seyfert 1 galaxies, we show that Narrow-Line Seyfert 1 galaxies (NLS1s) have larger ratios of 60μm-flux/1keV-flux. Using IRAS colors, we further make clear that these higher ratios are due to excess contributions of star formation activities to 60μm-flux densities rather than excess AGN contributions there. It is also shown with an X-ray luminosity limited sample that the result is not due to X-ray faintness of NLS1s compared to Broad-Line Seyfert 1 galaxies (BLS1s). It has been suggested from permitted line width, spectral energy distributions and time variability of NLS1s that they have relatively smaller black-hole masses and larger luminosity–to–Eddington luminosity ratios compared to those of BLS1s. Then, our results are naturally explained by a hypothesis in which some trigger (e.g., galaxy-galaxy merging) causes both starburst and gas fueling in the nucleus: luminosity of star formation will be fading after a sudden rise at the epoch of the merging, while that of active nucleus will rise gradually even after the epoch due to increasing Eddington limit with increasing black-hole mass. A number of studies of NLS1s to date have mainly focused on their extreme physical states of the central engine. We here propose that NLS1s are interesting objects for the formation and evolution of the active nuclei as well.

1. Introduction

Narrow-Line Seyfert 1 galaxies (NLS1s) belong to a peculiar subclass of Active Galactic Nuclei (AGNs) characterized by following factors (see Pogge 2000): (i) their relatively narrower Balmer lines of hydrogen (e.g., FWHM of Hβ $\lesssim$ 2000 km/s) (e.g., Osterbrock & Pogge 1985). They indeed belong to Seyfert 1 in terms of [OIII] 5007 Å to Hβ flux ratios. (ii) They often emit strong FeII multiplets and higher ionization iron lines, that are seen in Seyfert 1s but not seen in Seyferts 2s (e.g., Halpern & Oke 1987). The fraction of NLS1s among Seyfert 1s is about 10–50% depending on relevant wavebands and selection criteria.

Provided that the width of broad component in Balmer lines simply represents the virial velocity at Broad Line Region (BLR), FWHM of Hβ will be proportional to $(M_{\rm BH}/R_{\rm BLR})^{1/2}$, where $M_{\rm BH}$ and $R_{\rm BLR}$ are the mass of the central black-hole and a distance of representative broad line clouds measured from the black-hole, respectively. Then, the relatively narrower Balmer lines seen in NLS1s can be interpreted as signatures of smaller $M_{\rm BH}$ (with similar $R_{\rm BLR}$) and/or larger $R_{\rm BLR}$ (with similar $M_{\rm BH}$).

The hotter UV–soft X-ray bump of NLS1s compared with those of BLS1s/QSOs is another remarkable feature. A representative example of the spectral energy distribution (SED) of a NLS1 is obtained for Mrk 478 (Marshall et al. 1996) showing its spectral peak at $\sim$ 200 Å, while bright QSOs having their peak at 1000–2000 Å (Zheng et al. 1997; Laor et al. 1997). In the context of accretion disks, such a hotter, but still luminous ($10^{10-12}L_\odot$), big bump is achieved by smaller $M_{\rm BH}$ and larger $L/L_{\rm Edd}$, where $\dot{M}$, L and $L_{\rm Edd}$ are the mass accretion rate, bolometric luminosity of the nuclei ($L \sim 0.1\dot{M}c^2$) and Eddington luminosity [$\sim 10^{46}(M_{\rm BH}/10^8M_\odot)\,{\rm erg\ s^{-1}}$], respectively. That is because the maximum temperature of the standard accretion disk, $T_{\rm max}$, is $T_{\rm max} \propto {M_{\rm BH}}^{-1/2}\,\dot{M}^{1/4} \propto {M_{\rm BH}}^{-1/4}(\dot{M}/L_{\rm Edd})^{1/4}$. Model fitting for soft X-ray excess components of NLS1s also indicates their small $M_{\rm BH}$ and large $L/L_{\rm Edd}$ (Hayashida 2000).

Time variability provides two more noticeable features of NLS1s. First, rapid soft/hard X-ray variability is a distinguishing characteristic of NLS1s (e.g., Otani et al. 1996; Leighly 1999). A series of analysis of the short-term variability using the power spectral density shows that NLS1s have smaller $M_{\rm BH}$ (Hayashida 2000). Another estimations of $M_{\rm BH}$ with reverberation mapping technique again indicates smaller $M_{\rm BH}$ in NLS1s (Wandel et al. 1999). PG QSOs with relatively smaller $M_{\rm BH}$ also show narrower Hβ (Kaspi et al. 2000).

To summarize the three features above (Balmer line width, SED and time variability), the most promising picture of NLS1s is that they contain relatively less massive black-holes (with $M_{\rm BH} \sim 10^{5-7}M_\odot$) and higher $L/L_{\rm Edd}$ (with $L \sim L_{\rm Edd}$). In other words, their black-holes have not yet fed so much; they may be in early phase of AGN formation. If that is the case, NLS1s are likely to be the key objects to solve the question: what causes the gas fu-

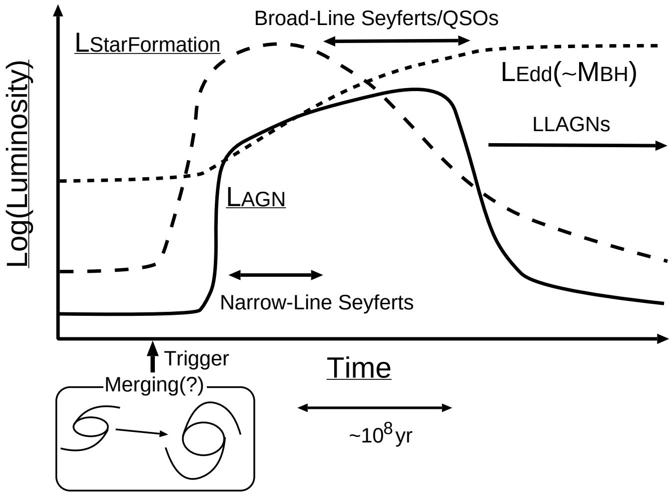

Fig. 1. A schematic view of our scenario: After some event triggering both star formation and AGN activities, NLS1s would appear in the earlier phase, while BLS1s/QSOs are objects in the latter phase of the AGN formation. When gas fueling stops, such objects will be identified as Low-Luminosity AGNs.

eling in AGNs. The surrounding gas can be channeled into the nuclei by a strong non-axisymmetric perturbation, e.g., galaxy-galaxy merging/interaction, which will also results in an enhanced star formation activities in their host galaxies (e.g., Mihos & Hernquist 1996). Throughout this study, we adopt H_0 of 75 km/s/Mpc and q_0 of 0.5.

2. Scenario, Sample and Data

2.1. Proposed Scenario

A working hypothesis throughout this paper is as follows (figure 1). Consider that some perturbation on a galaxy, e.g., galaxy-galaxy interaction/merging, triggers activities both of star formation and AGN activities. Star formation luminosity will rise immediately and gradually decay (dashed curve). Since $M_{\rm BH}$ is small in earlier phase, $L_{\rm Edd}$ ($\propto M_{\rm BH}$) is also small (dotted curve). As a result, AGN luminosity ($\lesssim L_{\rm Edd}$) will rise gradually over the life time of the AGN activity ($\sim 10^8$ yr; solid line). The e-folding timescale for evolution of $M_{\rm BH}$, $t_{\rm Edd}$, in the case of the Eddington luminosity is evaluated as $t_{\rm Edd} \equiv M_{\rm BH}/\dot{M}_{\rm Edd} = 3.7 \times 10^7$ yr, where, $\dot{M}_{\rm Edd} \equiv L_{\rm Edd}/(\eta c^2)$. Here, η is the conversion efficiency of gravitational energy into radiative energy, and taken to be 1/12. In the slim disk regime, which is presumably realized in NLS1s, the efficiency η becomes to decrease (Abramowicz et al. 1988; Mineshige et al. 2000), and the evolution timescale can be shorten.

What we would expect from this scenario is that the ratio of star formation luminosity over AGN luminosity should differ between NLS1s and BLS1s; higher ratios preferentially in NLS1s. Thus, in what follows, we are going to search evidences confirming the scenario, focusing on the ratios as functions of FWHM of broad component of Hβ lines.

Here, we wish to stress on the following fact that star formation and AGN activities show different dependencies of luminosities upon gas concentration. It is known that the higher the gas concentration is, the higher star formation activity becomes (Kennicutt 1998). On the other hand, the AGN luminosity has less dependence upon gas concentration towards the center. In fact, the luminosity of accretion disk L is believed to be in a limited range; $0.01 L_{\rm Edd} \lesssim L \lesssim L_{\rm Edd}$. The upper limit comes from the fact that L becomes to saturate around $L_{\rm Edd}$ when the mass accretion rate exceeds over $\dot{M}_{\rm Edd}$ because of the advection within the flow (Abramowicz et al. 1988). Namely, luminous QSOs, harboring massive black-holes ($10^{8-9} M_{\odot}$), were fainter before in their earlier (younger) phases. The lower limit is due to the transition from the standard disk, where $\eta \sim 0.1$, to the optically thin advection dominated flow, in which $\eta \ll 0.1$ (Narayan & Yi 1995), when the accretion rate is much less than $0.01 \dot{M}_{\rm Edd}$.

2.2. Luminosities of Star Formation and AGN

How extent a galaxy contains ongoing star formation activity can be well evaluated from its Far-Infrared (FIR) radiation originated to dust emission around massive stars. We use flux densities at 60μm ($f_{60\mu{\rm m}}$) from IRAS data. Most of the data are taken from the IRAS Faint Source Catalog (Moshir et al. 1990), Catalog of Infrared Observations (Gezari et al. 1999) and Grupe et al. (1998; hereafter G98).

Flux densities at 1 keV ($f_{\rm 1keV}$) measured by ROSAT are used for the representative luminosities of AGNs. The integrated fluxes or flux densities at 2 keV were converted into $f_{\rm 1keV}$. In some objects that were observed by ROSAT All-Sky Survey (RASS) and pointing observations, the latter data are preferentially used for this analysis due to their better signal-to-noise ratios.

2.3. Basic Quantities of the Sample

Objects used in this study are those which have data of FWHM of Hβ, 1 keV and 60μm flux densities. These objects are chosen from Boller et al. 1996 (hereafter BBF96), Walter and Fink 1993 (WF93), I Zw 1 objects, Seyfert 1s and 1.5s in Moran et al. 1996 (MHH96), and G98/Grupe et al. 1999 (G99).

In total, we have 144 objects with the data. The basic quantities of the sample are as follows: 60μm-luminosities ($L_{60\mu{\rm m}}$) are between $10^{42.5}$ and $10^{46.5}$ erg/s, 1keV-luminosities ($L_{\rm 1keV}$) between $10^{40.5}$ and 10^{45} erg/s and redshifts from 0.002 to 0.7. The $L_{\rm 1keV}$ distribution is quite different between broader and narrower objects; high-$L_{\rm 1keV}$ objects are rare in the narrower half. This can be interpreted by the Eddington limit which will be proportinal to FWHM^4 if we assume that $R_{\rm BLR} \propto L^{1/2}$, $L \propto \dot{M}$ and FWHM $\propto (M_{\rm BH}/R_{\rm BLR})^{1/2}$. On the other hand, the $L_{60\mu{\rm m}}$ distributions are almost similar

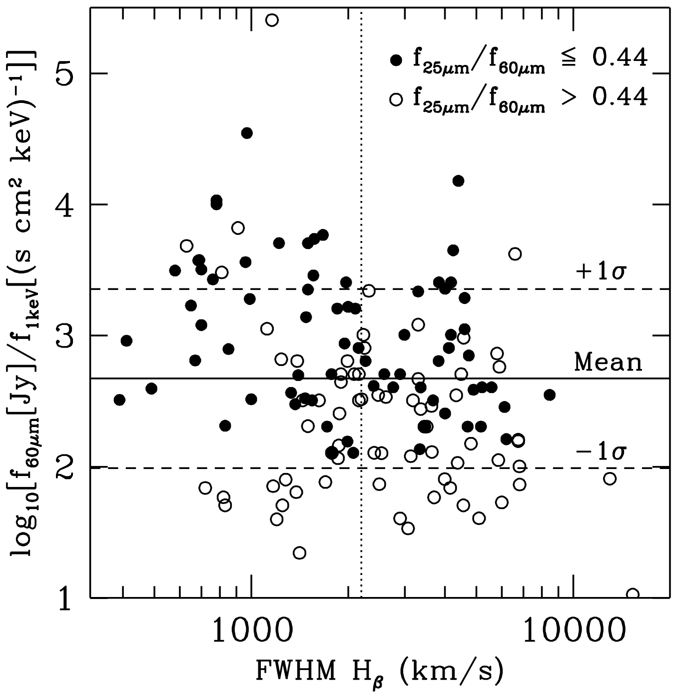

Fig. 2. The ratios of flux density at 60μm to that at 1 keV as functions of FWHM of broad component in Hβ emissions.

in broader and narrower samples. We have confirmed through Kolmogorov-Smirnov tests (K-S tests; Press et al. 1992) that there is no serious selection bias between broader and narrower objects in terms of $L_{60\mu m}$ and redshifts.

3. Results

Figure 2 shows the main result: the ratios of flux densities at 60μm to those at 1 keV as functions of FWHM of broad component in Hβ emissions. Filled circles denote relatively cooler IRAS sources ($f_{25\mu m}/f_{60\mu m} \leq 0.44$), while open circles represent relatively warmer sources. Here, $f_{25\mu m}/f_{60\mu m} = 0.44$ is the median among the whole sample. When only upper limits of $f_{25\mu m}$ are available (23/144), we used the upper limits of $f_{25\mu m}$ as the true values for the present. It is known that $f_{25\mu m}/f_{60\mu m}$ of about 0.2–0.3 is the boarder line between galaxies with nuclear H II regions and AGNs (de Grijp et al. 1987). Lower value of $f_{25\mu m}/f_{60\mu m}$ indicates more contribution of star formation activities in FIR radiation. Horizontal solid line indicate the mean value of the logarithm of the flux density ratios (2.67), and dashed lines represents its standard deviation (± 0.68). Vertical dotted line at FWHM = 2200km/s is the median of FWHM of Hβ for the whole objects.

We wish to stress that objects with higher ratios (e.g., $\gtrsim 10^3$) preferentially lie in the narrower half. Indeed, the fractions of objects with $\log(f_{60\mu m}/f_{1\mathrm{keV}}) >$ mean + 1 σ in each half is 26% (19/72) and 8% (6/72) in the narrower and broader halves, respectively. In order to make further statistical statements, we applied the K-S tests for distributions of $\log_{10}(f_{60\mu m}/f_{1\mathrm{keV}})$ in narrower and broader samples with various threshold values for FWHM of H_β (1500, 1600,..., 2500 km/s). The probability that the two distributions are drawn from the same population changes from 0 to 4%. The least, and thus most significant, probability is achieved (0.18%) when we divide the objects at FWHM = 1700 km/s.

There are three possible reasons to result in the higher ratios of NLS1s: i) excess contributions to $f_{60\mu m}$ from AGN luminosities (e.g., enhanced radiation from dusty tori), ii) excess contributions to $f_{60\mu m}$ from star formation luminosities (i.e., starburst), and iii) strong X-ray time variability in narrower H_β objects (i.e., reduced $f_{1\mathrm{keV}}$).

First of all, our result is consistent with the study by MHH96 who showed a trend that NLS1s have higher $L_{\mathrm{FIR}}/L_{\mathrm{X-ray}}$ ratios (e.g., Halpern & Oke 1987; but see also Polletta & Courvoisier 1999). However, it was not clear whether the higher ratios are due to (i) or (ii). The IRAS color denoted in figure 2 tells that cooler objects tend to have higher ratios, whereas warmer objects have lower ratios. This shows that excess AGN contribution to $f_{60\mu m}$ (i) is rejected as the reason behind the higher ratios of narrower objects and that higher star formation activity (ii) is preferred.

Next, extreme (a factor of 10–100) X-ray time variabilities have been reported in some NLS1s: short-term ($\lesssim$ day) variabilities in IRAS 13224-3809 and PHL 1092, as well as long-term ($\gtrsim$ year) variabilities in NGC 4051, RE J1237+264 (= IC 3599), WPVS 007, and RX J0134.2-4258. Four objects among them are included in our sample. If we use the data during X-ray low-states instead of those in high-states, the ratios become higher by an order of $\sim (1-2)$, and vice versa. The IRAS color seems to again rule out this explanation (iii). If the higher ratios of NLS1s are due to their being low-$f_{1\mathrm{keV}}$ state during the ROSAT observations by chance, these objects should include both cool and warm objects since IRAS colors during IRAS mission (in 1980's) are unlikely to correlate with the $f_{1\mathrm{keV}}$ faintness during the ROSAT mission (in 1990's).

It should be noted here that Mathur (2000) reached a similar scenario in the context of gas content and metal richness of NLS1s. Also, Grupe (1996) mentioned that the age of AGNs might be a possible reason behind several features of NLS1s.

One may think that our primary finding (figure 2) is due to low $L_{1\mathrm{keV}}$ of NLS1s (§2.3). With the X-ray luminosity-limited ($10^{41.5} < L_{1\mathrm{keV}} < 10^{44}$ erg/s) sample including 121 objects, we conclude that the results are not due to the X-ray faintness of NLS1s. The flux density ratios v.s. FWHM relations for this luminosity-limited sample exhibits a similar distribution in a sense that higher-ratio objects with cooler IRAS colors tend to belong to the narrower half. In other words, high-ratios of $f_{60\mu m}/f_{1\mathrm{keV}}$ in NLS1s are results of high star formation activities in such objects, rather than the X-ray faintness of NLS1s.

These findings are consistent with our hypothesis in which NLS1s are in earlier phase of AGN evolution accompanied with enhanced star formation activities, whereas BLS1s (and probably QSOs as well) are the evolved objects due to mass accretion to the central black-hole with faded star formation.

4. Summary

We show through an analysis with 144 Seyfert 1 galaxies that Narrow-Line Seyfert 1 galaxies (NLS1s) have large luminosity ratios of star formation to active nuclei, which are replaced by $f_{60\mu m}$–to–$f_{1\rm keV}$ ratios in the present study. The result above is consistent with study by Moran et al. (1996). We further make clear using IRAS colors that the higher ratios are due to excess contributions of star formation activities to $f_{60\mu m}$ rather than excess AGN contributions. It is also shown that the result is not due to the lack of luminous X-ray objects in NLS1s compared to Broad-Line Seyfert 1 galaxies (BLS1s); an X-ray luminosity-limited ($10^{41.5} < L_{1\rm keV} < 10^{44}$ erg s^{-1}) sample shows a similar distribution in a sense that higher-ratio objects with cooler IRAS colors tend to belong to NLS1s.

Our results are naturally explained by a hypothesis in which some trigger (e.g., galaxy-galaxy merging) causes both starburst and gas fueling in the nucleus: luminosity of star formation ($L_{60\mu m}$) will decrease after a sudden rise at the epoch of the merging, while that of active nucleus ($L_{1\rm keV}$) will rise gradually even after the epoch due to increasing Eddington limit with increasing black-hole mass.

A number of studies of NLS1s to date have mainly focused on their extreme physical states of the central engine (e.g., accretion disks/flows, line-emitting regions, absorbing materials, inclination of accretion disks). We here propose that NLS1s are interesting objects for the formation/evolution of the active nuclei and supermassive black-holes as well. More details will be presented elsewhere (Kawaguchi & Aoki 2000).

5. Future Direction

The main cause of gas fueling in nuclei has been studied in some decades. A possible mechanism is the galaxy-galaxy merging/interaction. One of the major claims against this hypothesis will be that only 10-30% of Seyferts show close companion galaxies (e.g., Rafanelli et al. 1995; De Robertis et al. 1998). Also, gas fueling induced by bar structure is still controversial (e.g., Regan & Mulchaev 1999; Knapen et al. 2000). Here, we wish to point out that these fractions are basically derived from samples selected so as to include luminous objects. However the babies of Seyferts/QSOs, which are probably NLS1s, are likely to be fainter than BLS1s and QSOs (e.g., Marshall et al. 1996). We argue that NLS1s (rather than bright Seyferts/QSOs) are the key objects to know how central gas fueling is triggered.

Acknowledgements. TK thanks JSPS Research Fellowships for financial supports.

References

Abramowicz M.A., Czerny B., Lasota J.P. & Szuszkiewicz E., 1988. ApJ, 332, 646
Boller Th., Brandt W.N., Fink H.H. 1996, A&A 305, 53 (BBF96)
de Grijp M.H.K., Miley G.K. & Lub J. 1987, A&A Suppl., 70, 95
De Robertis M.M., Yee H.K.C. & Hayhoe K. 1998, ApJ, 496, 93
Gezari D.Y., Pitts P.S., Schmitz M. 1999, Catalog of Infrared Observations, Edition 5,
Grupe D. 1996, Ph.D. Thesis, Göttingen University
Grupe D., Beuermann K., Thomas H.-C., Mannheim K. Fink H.H. 1998, A&A 330, 25 (G98)
Grupe G.D., Beuermann K., Mannheim K., Thomas H.-C. 1999, A&A 350, 805 (G99)
Halpern J.P., Oke J.B. 1987, ApJ 312, 91
Hayashida K. 2000, New Astronomy Reviews, 44, 419
Kaspi S., Smith P.S., Netzer H., Maoz D., Jannuzi B.T. & Giveon U. 2000, ApJ, 533, 631
Kawaguchi T. & Aoki K. 2000, submitted to PASJ
Kennicutt Jr., R.C. 1998, ApJ, 498, 541
Knapen J.H., Shlosman I. & Peletier R.F. 2000, ApJ, 529, 93
Laor A., Fiore F., Elvis M., Wilkes B.J., McDowell J.C. 1997, ApJ 477, 93
Leighly K.M. 1999, ApJS, 125, 297
Marshall H.L., Carone T.E., Shull J.M., Malkan M.A. & Elvis M. 1996, ApJ, 457, 169
Mathur S. 2000, MNRAS, 314, L17
Mihos J.C. & Hernquist L. 1996, ApJ, 464, 641
Mineshige S., Kawaguchi T., Takeuchi M. & Hayashida K. 2000, PASJ, 52, 499
Moran E.C., Halpern J.P. & Helfand D.J. 1996, ApJS, 106, 341 (MHH96)
Moshir M. et al. 1990, IRAS Faint Source Catalog, ver. 2.0
Narayan R. & Yi I. 1995, ApJ, 452, 710
Osterbrock D.E., & Pogge R.W. 1985, ApJ, 297, 166
Otani C., Kii T., Miya K. 1996 in Röntgenstrahlung from the Universe (MPE Report 263), ed H.U. Zimmermann, J.E. Trümper, H. Yorke (MPE Press, Garching) p491
Pogge R.W. 2000, New Astronomy Reviews, 44, 381
Polletta, M. & Courvoisier, T.J.-L. 1999, A&A, 350. 765
Press W. H., Teukolsky S. A., Vetterling W. T. & Flannery B. P., 1992, Numerical Recipes: The Art of Scientific Computing, 2nd Edition (New York: Cambridge Univ. Press) §14.3
Rafanelli P., Violato M., & Baruffolo A. 1995, AJ, 109, 1546
Regan M.W. & Mulchaev J.S. 1999, AJ, 117, 2676
Walter R. & Fink H.H. 1993, AA, 274, 105 (WF93)
Wandel A., Peterson B.M. & Malkan M.A. 1999, ApJ, 526, 579
Zheng W., Kriss G.A., Telfer R.C., Grimes J.P. & Davidsen A.F. 1997, ApJ, 475, 469